

Indirect band-gap transitions in GaP shocked along the [100], [110], and [111] axes

P. Grivickas, M. D. McCluskey, and Y. M. Gupta

Institute for Shock Physics and Department of Physics and Astronomy, Washington State University, Pullman, Washington 99164-2816, USA

(Received 7 January 2007; revised manuscript received 19 April 2007; published 29 June 2007)

Shock compression experiments were performed to investigate optical changes in GaP under uniaxial strain. Low-temperature transmission spectra of sulphur-doped GaP samples were obtained at longitudinal stresses up to 5 GPa for shock wave loading along the [100], [111], and [110] orientations. At low uniaxial strains, changes in the band-gap absorption edge were consistent with the calculated band-gap shifts using the published deformation potentials. At high uniaxial strains, however, the published deformation potentials overestimated the shifts. This observation was confirmed by photoluminescence spectroscopy of S bound excitonic lines in shocked GaP:S. In addition, at strains higher than a few percent, a reduction in the intrinsic excitonic contribution to the band-gap absorption was obtained by modeling the absorption data with indirect-transition theory.

DOI: [10.1103/PhysRevB.75.235207](https://doi.org/10.1103/PhysRevB.75.235207)

PACS number(s): 71.55.Eq, 71.70.Fk, 62.50.+p, 78.40.-q

I. INTRODUCTION

A detailed understanding of band-gap transitions in gallium phosphide (GaP) is important for a variety of optoelectronic applications based on this III-V semiconductor and its alloys. The application of external stress is a powerful approach to investigate the intrinsic properties of the electronic bands responsible for these transitions. GaP has been studied extensively through the application of uniaxial stress and hydrostatic pressure. Uniaxial stress causes biaxial strain, thereby reducing the cubic symmetry of zinc-blende GaP. This technique was used to determine the deformation potentials of direct and indirect band states,¹ reveal the detailed structure of the indirect band edge,² and identify the symmetry and the ionization energies of substitutional dopants,^{3,4} isoelectronic impurities,⁵⁻⁷ and defect complexes.⁸ Due to the low elastic limit of single crystals, however, the magnitude of uniaxial stress in GaP was usually below a one GPa limit. This range was extended to tens of GPa by applying hydrostatic pressure in diamond anvil cells (DACs). The isotropic strain achieved in DAC experiments further elucidated the interactions between direct and indirect states⁹ and the nonlinear behavior of excitons bound to isoelectronic traps and their complexes.¹⁰ Hydrostatic pressure, however, does not lift the degeneracy of electronic states in GaP, concealing many important properties. Further insights into the nature of band structure of GaP can be obtained combining symmetry breaking and high stresses in a single experiment.

Shock wave experiments create conditions of uniaxial strain along the wave propagation direction. This deformation reduces the symmetry in a crystal and exhibits a much higher elastic limit as compared to biaxial strain.^{11,12} The advantages of shock wave compression were recently demonstrated for a study of deformation potentials of GaN.¹³ In this work, we examined the reported deformation potentials for band-to-band transitions in uniaxially strained GaP. At large strains, we detected deviations from the predictions based on the published deformation potentials. In addition, we observed a substantial decrease in the intrinsic excitonic contribution to the absorption edge.

II. THEORY

Band structure changes and related indirect transitions of GaP for biaxial strain were analyzed in several papers.^{2,14,15} The most comprehensive set of deformation potentials (DPs) is provided in Ref. 1; we have used the same notation. Descriptions of the DPs and their values are provided in Table I.

At ambient conditions, the indirect band gap of GaP originates from the maximum of the Γ_8 valence band (VB) and the minimum of the conduction band (CB) close to the X_6 symmetry point at the zone boundary. Under nonisotropic strain, the fourfold degenerate multiplet of the VB and the three equivalent valleys of the CB split into several subbands. This splitting is illustrated in Fig. 1 for compressive strain oriented along the [100], [111], and [110] directions. In all three orientations, the VB splits into two components VB1 and VB2. The CB splits into two subbands CB1 and CB2 for the [100] and [110] directions. We also consider the lower valence band VB3, separated by $\Delta_0=90$ meV due to crystalline spin-orbit coupling, which affects the band-gap absorption edge at large strains.

The individual transitions I_k resulting from the described subbands are shown in Fig. 1 for three orientations. The energies of these transitions shift under applied stress according to the dependencies provided in Table II. In the case of shock compression, the X deformations are directly proportional to the uniaxial strain e_1 along the crystallographic axis parallel

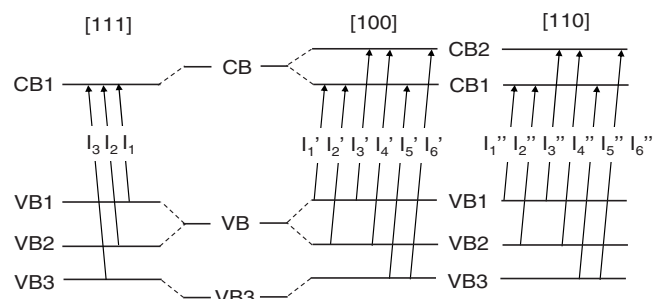


FIG. 1. Schematic illustration of split subbands and corresponding transitions in GaP strained along different crystallographic axes.

TABLE I. Deformation potentials (DPs) of GaP and their values according to Ref. 1.

DP	Value (eV)	Description
$E_1+a_1+a_2$	2.3 ± 0.5	Hydrostatic DP of CB (E_1) and VB (a_1+a_2)
a_2	-0.4 ± 0.3	Hydrostatic DP of VB due to spin-orbital interactions
$E_1+a_1-3a_2$	3.5 ± 0.8	Hydrostatic DP of CB and VBb
E_2	6.3 ± 0.9	Shear DP of CB
E_3	13 ± 1.5	Shear DP of CB due to X_6 and X_7 coupling
b_1+2b_2	-1.5 ± 0.2	
b_1-b_2	-2.1 ± 0.3	Shear DPs of VB and VBb due to orbital (b_1, d_1)
d_1+2d_2	-4.6 ± 0.2	and spin-orbital (b_2, d_2) interactions
d_1-d_2	-5.5 ± 0.2	
Δ_0	0.09 ± 0.01	Energy difference between VB and VBb ($\Gamma_8-\Gamma_7$)
δ	0.5 ± 0.05	Energy difference between CB minimum in X_6 band and higher conduction band X_7

to the applied longitudinal stress. The e_1 strain is obtained from the known longitudinal stress σ and the appropriate elastic constants. For the sake of consistency with Ref. 1, we use the same set of elastic constants $C_{11}=141.3$ GPa, $C_{12}=62.68$ GPa, and $C_{44}=70.47$ GPa.¹⁶ These values are within 1% of the average of reported data for GaP.¹⁷ The shift of the transitions versus e_1 , calculated according Table I, is shown in Fig. 2. We use the convention that positive e_1 values indicate compressive strain.

III. EXPERIMENTS

The [100], [111], and [110] GaP:S samples used in this study had sulphur concentrations of 7×10^{17} , 12×10^{17} , and 8×10^{17} cm⁻³ at room temperature, respectively. To evaluate the possible effect of doping levels, the [100] orientation transmission measurements were also carried out on a low-doped (2×10^{15} cm⁻³) sample. Figure 3 shows absorption spectra of the samples at ambient pressure and liquid nitrogen temperature (77 K). Due to thermal broadening effects, low temperatures are essential to reveal the detailed structure of absorption spectra for indirect band-gap semiconductors. At low photon energies, all spectra exhibit a roughly constant

absorption that may originate from transitions from donor and donor-complex states within the band gap.¹⁸ At ~ 2.33 eV the constant absorption is overtaken by the intrinsic absorption edge of GaP. The peak at ~ 2.3 eV is due to S bound excitons (S:BEx).¹⁹ The second peak in the doped [100] sample, at a higher energy (2.313 eV), arises from unintentional nitrogen doping.²⁰

GaP:S band-gap states were studied as a function of uniaxial strain using time-resolved optical transmission measurements in shock-wave experiments.¹³ The experimental configuration is shown schematically in Fig. 4. A 15×15 mm sample was cut from a 400–500 μ m thick GaP:S wafer and glued by optically transparent epoxy (< 2 μ m thickness bond) onto a c -cut sapphire buffer window. This target was mechanically attached to an aluminum holder while cooling the system with liquid nitrogen. The thermal expansion coefficients for GaP and sapphire are similar such that the strain due to cooling was negligible. A shock wave in the target was produced by an impactor window (c -cut sapphire, z -cut quartz, or PMMA) mounted on a projectile and accelerated by a gas gun. Collimated light from a xenon flashlamp was reflected by two turning mirrors on the projectile, transmitted through a 3 mm diameter aperture onto the impactor-GaP-buffer arrangement, and focused into an

TABLE II. Shifts of indirect band-gap transitions in uniaxially strained GaP with respect to the ambient band-gap.

	[100]	[111]	[110]
Transitions	$I_1' = A_x - B + \frac{2}{3}G - 2B'^2/(\Delta_0' + B)$ $I_2' = A_x + B + \frac{2}{3}G$ $I_3' = A_x - B - \frac{1}{3}G - 2B'^2/(\Delta_0' + B)$ $I_4' = A_x + B - \frac{1}{3}G$ $I_5' = A_0 + \frac{2}{3}G + 2B'^2/(\Delta_0' + B)$ $I_6' = A_0 - \frac{1}{3}G + 2B'^2/(\Delta_0' + B)$	$I_1 = A_x - D - 2D'^2/(\Delta_0' + D) - \frac{1}{9}H^2/\delta$ $I_2 = A_x + D - \frac{1}{9}H^2/\delta$ $I_3 = A_0 + 2D'^2/(\Delta_0' + D) - \frac{1}{9}H^2/\delta$	$I_1'' = A_x - F + \frac{1}{6}G - 2F'^2/(\Delta_0' + F) - \frac{1}{4}H^2/\delta$ $I_2'' = A_x + F + \frac{1}{6}G - \frac{1}{4}H^2/\delta$ $I_3'' = A_x - F - \frac{1}{3}G - 2F'^2/(\Delta_0' + F) - \frac{1}{4}H^2/\delta$ $I_4'' = A_x + F - \frac{1}{3}G - \frac{1}{4}H^2/\delta$ $I_5'' = A_0 + \frac{1}{6}G + 2F'^2/(\Delta_0' + F) - \frac{1}{4}H^2/\delta$ $I_6'' = A_0 - \frac{1}{3}G + 2F'^2/(\Delta_0' + F) - \frac{1}{4}H^2/\delta$
Components	$A_x = (E_1 + a_1 + a_2)X_1$; $A_0 = (E_1 + a_1 - 2a_2)X_1$; $B = (b_1 + 2b_2)X_2$; $G = E_2X_2$; $B' = (b_1 - b_2)X_2$; $\Delta_0' = \Delta_0 - 3a_2X_1$; $D = [(d_1 + 2d_2)/2\sqrt{3}]X_3$; $D' = [(d_1 - d_2)/2\sqrt{3}]X_3$; $H = (E_3/2)X_3$; $F = (B + 3D)/4$; $F' = (B' + 3D')/4$		
Deformations	$X_1 = X_2 = e_1' = \sigma/C_{11}$	$X_1 = X_3/2 = e_1 = 3\sigma/(C_{11} + 2C_{12} + 4C_{44})$	$X_1 = X_2 = X_3/2 = e_1'' = 2\sigma/(C_{11} + C_{12} + 2C_{44})$

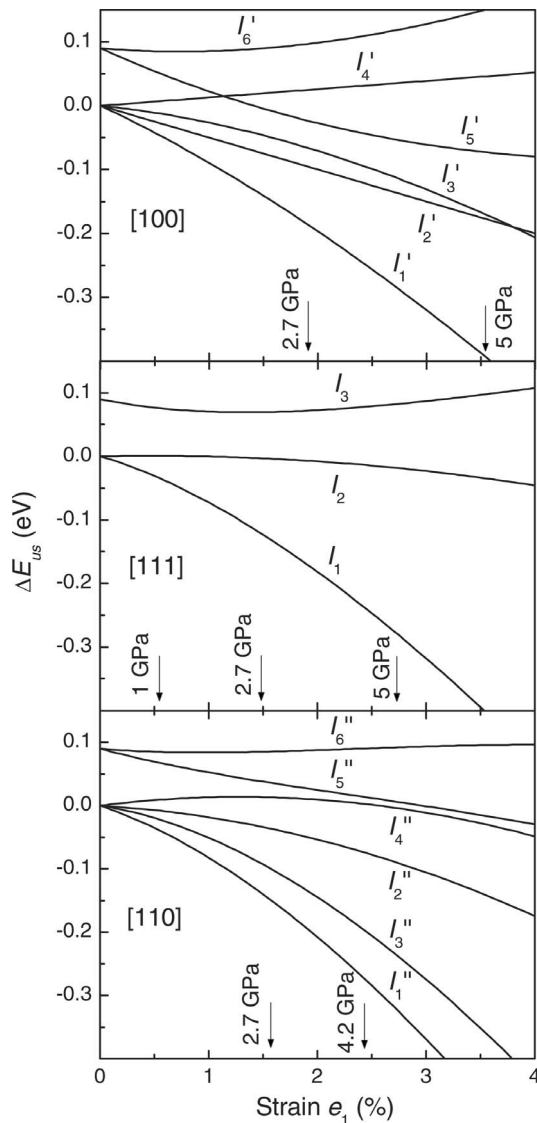


FIG. 2. Band gap changes in GaP uniaxially strained along [100], [111], and [110] orientations, according to the published deformation potentials (Tables I and II).

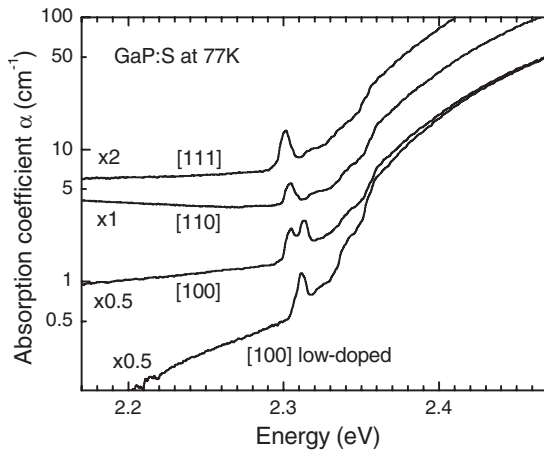


FIG. 3. Spectra of GaP:S samples at ambient pressure (liquid nitrogen temperature).

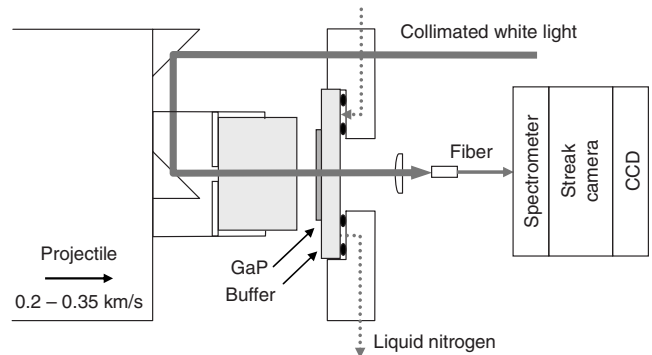


FIG. 4. Schematic diagram of transmission measurements in shock-wave experiments.

optical fiber. Light from the collecting fiber was spectrally dispersed by an imaging dual-grating spectrometer, temporally dispersed by an electronic streak camera (Cordin), and digitally recorded by a charge-coupled device (CCD) array. The time resolution of the system was ~ 20 ns.

The streak camera operates by directing electrons generated on a photocathode onto the output phosphorescing screen through a vacuum tube.²⁰ Within the vacuum tube, however, some of the electron beam gets scattered and induces a background signal, as shown in the inset of Fig. 5 for the case of a partially covered photocathode. This effect results in spectral broadening, as shown in Fig. 5 for the absorption spectrum of a [111] GaP:S sample taken with a scanning spectrometer (diamond symbols) and a streak camera (circle symbols). To account for this effect, we used a convoluting function to reproduce the light-induced background (Fig. 5, inset). The solid line in Fig. 5 represents the scanning spectrometer data recalculated using this function and good agreement is observed with the streak camera spectrum. The same convolution function was used to model all the absorption data in this study.

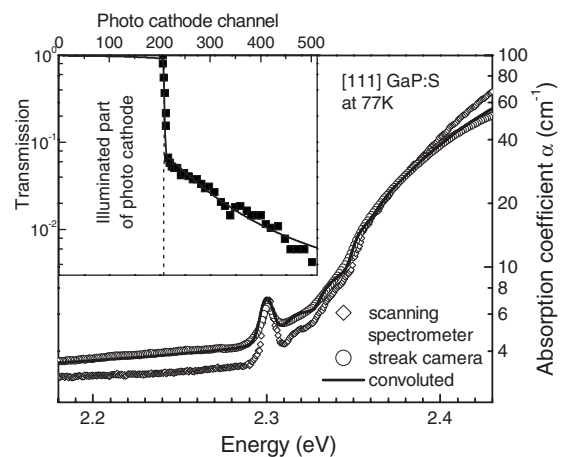


FIG. 5. Spectra of [111] GaP:S sample obtained with a scanning spectrometer (diamond symbols) and a streak camera (circle symbols). The solid line is a model of the absorption using the appropriate convolution function. The inset shows the spectral response of the streak camera with a partially covered photocathode, where the symbols are experimental data, and the line is a data fit using the convolution function.

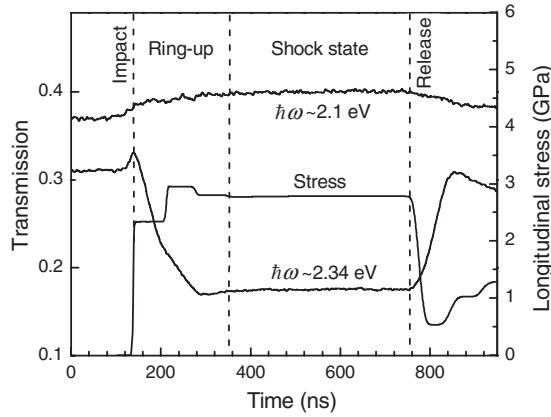


FIG. 6. Time evolution of longitudinal stress and transmission at two different photon energies in shock experiment on a quartz-[100]GaP-sapphire system, with a final longitudinal stress of 2.7 GPa.

The longitudinal stress within a sample was determined by the shock response of GaP and the window materials. Figure 6 shows the calculated²¹ stress dependence for a 480- μm -thick [100] GaP:S sample bonded to a 2.5-mm-

thick sapphire buffer, arising from impact by a 3.17-mm-thick quartz impactor with a velocity of 222 m/s. After an initial ring-up process, due to the impedance mismatch between the sample and the impactor/buffer materials, a constant stress state is reached. This stress persists until the arrival of a release wave from the nearest free surface. The stress value was calculated to an accuracy of few percent from the well-established shock velocities in *c*-cut sapphire,²² *z*-cut quartz,²³ and PMMA.²⁴ The corresponding²⁵ temporal changes in transmission during the shock experiment are illustrated in Fig. 6 for the spectral regions around 2.1 and 2.34 eV. Both curves exhibit a sharp increase in intensity at the moment of impact, due to the loss of one interface between the sample and impactor window. During the ring-up, the transmission changes along with the longitudinal stress. These changes are more pronounced at the intrinsic absorption edge of GaP (2.34 eV), due to the red shift of the band gap. After the final shock state is established, the transmission maintains a constant value for ~ 400 ns. All transmission data for shocked GaP were collected and averaged during this time window.

The absorption coefficient α at a photon energy $\hbar\omega$ is obtained from the transmission T according the expressions

$$\alpha = -(1/d) \ln \left(\frac{[(1-R_1)^2(1-R_2)^2 + 4R_1R_2T^2]^{1/2} - (1-R_1)(1-R_2)}{2R_1R_2T} \right), \quad T = \frac{(I-I_b)}{(I_0-I_b)}, \quad (1)$$

where d is the sample thickness, R_1 and R_2 are the reflection coefficients between the impactor-GaP and GaP-buffer interfaces, respectively, I is the intensity transmitted through the shocked sample, I_b is the background intensity recorded with the shutter of the streak camera closed, and I_0 is the reference intensity transmitted through the impactor and buffer. The reflection coefficients are calculated according to

$$R = \left(\frac{n_{\text{GaP}} - n_W}{n_{\text{GaP}} + n_W} \right)^2, \quad (2)$$

where n_{GaP} and n_W are the refractive indices of GaP and the window material, respectively.

IV. RESULTS

A. Luminescence of bound excitons

Figure 7 shows the calculated shifts of the I_1 and I_2 transitions for [111] GaP:S under uniaxial strain. The bounds of the calculations, indicated by the dashed areas, were obtained using the error range of the DPs specified in Table II. In the case of biaxial strain, it was demonstrated that the stress dependence of the lowest subband in GaP can be monitored directly by tracking the S:BEX peaks.⁴ In the present work, we detected the shift of S:BEX peaks in

shocked GaP:S by performing photoluminescence (PL) measurements using a 514.5 nm dye laser pulse as an excitation source. The obtained data were used to verify the accuracy of the published DPs. Detailed PL measurements of GaP will be presented elsewhere.

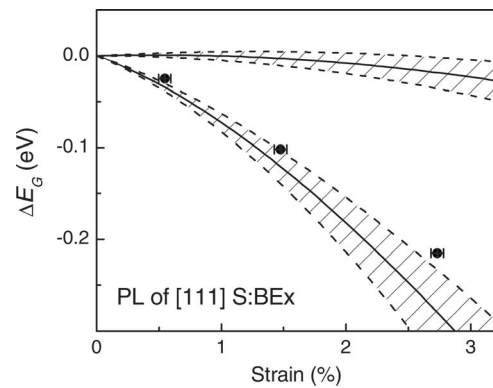


FIG. 7. Band gap changes in uniaxially strained [111] GaP:S. The solid lines represent the calculated averages while the dashed areas indicate the tolerance of calculation. The symbols are the experimental data representing the shift of S:BEX peak in the PL spectra of shocked GaP:S.

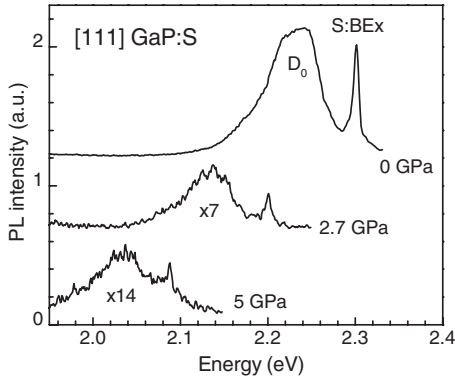


FIG. 8. PL spectra of [111] GaP:S at ambient conditions and for two shock stresses.

Figure 8 shows PL spectra of [111] GaP:S at ambient conditions and under shock compression at 2.7 and 5 GPa. The ambient spectrum showed a narrow S:BEx peak at 2.3 eV, and a broader peak at lower energies that arises from the recombination of free holes at neutral donor centers.²⁶ Under uniaxial strain, the intensity of the PL signal decreased, but remained sufficient to observe the redshift of both peaks. The S:BEx peak energies are plotted in Fig. 7. The figure shows that the experimental data differ from the calculated values. The same trend was also obtained for [100] and [110] GaP:S. In our model, therefore, we used the measured PL values for the lowest-energy transition (Table IV). For higher bands, the calculated values were used.

B. Band-gap absorption spectra

Figure 9 shows the absorption spectra for GaP:S shocked along the three principal crystallographic axes. All spectra show distinct red shifts with longitudinal stress. To emphasize the quadratic increase in absorption with photon energy, which is characteristic for indirect band-to-band transitions, the data are plotted as $\alpha^{1/2}$ versus energy. Under ambient conditions (gray curves), this results in a single linear slope above an initial structure due to the excitonic transitions. The shocked spectra, especially at [111] and [110] orientations, show, in contrast, few regions with distinct slopes, indicating the involvement of several subbands in the absorption shape of uniaxially strained GaP.

The presence of S:BEx peaks in the shocked spectra is clearly evident at a stress of 1 GPa in [111] GaP:S. The 2.24–2.34 eV spectral region is magnified in the inset of Fig. 9, showing a good match between the S:BEx peaks in absorption and PL spectra. At higher stresses, however, the S:BEx absorption peaks could not be detected, apparently due to the loss of oscillator strength (see the decreasing PL peak intensities at high stresses in Fig. 8) and the spectral broadening as discussed in the experiment part.

The flat absorption profile at low energies, due to the donor states within the band gap, shows a tendency to decrease slightly with increasing stress. In order to evaluate the effect of doping on the absorption profile, the 2.7 GPa experiment in [100] GaP was repeated for the low-doped sample. The difference between the spectra obtained for the two samples

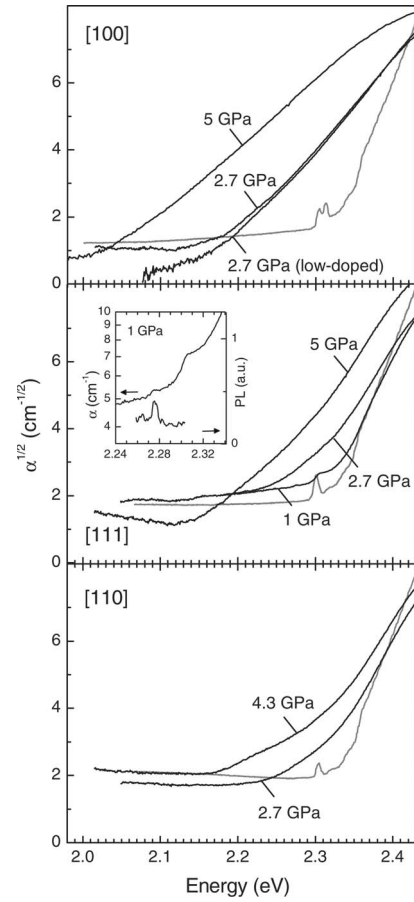


FIG. 9. Indirect absorption edge of shocked GaP at different crystallographic orientations and different longitudinal stresses.

is notable only at the low energy side (Fig. 9). As discussed in the next section, this small difference can be accounted for by adding a constant absorption level to the simulated spectrum.

C. Modeling

The absorption edge of indirect band-gap semiconductors is well explained by indirect optical transition theory.^{27,28} The theory implies that the basic shape of the absorption spectrum can be modeled using the following two contributions:

$$\alpha_k = \left(n_B + \frac{1}{2} \pm \frac{1}{2} \right) \left(C_{\text{ex}}^k \sum_p A_{\text{ex}}^p [\hbar\omega - (E_G - E_{\text{ex}} + \Delta E_{\text{dop}} + \Delta E_{\text{US}}^k \pm E_p)]^{1/2} + C_{\text{BB}}^k \sum_p A_{\text{BB}}^p [\hbar\omega - (E_G + \Delta E_{\text{dop}} + \Delta E_{\text{US}}^k \pm E_p)]^2 \right), \quad (3)$$

where $n_B = [\exp(E_p/k_B T) - 1]^{-1}$ is the phonon population, the p index labels a particular phonon branch with energy E_p , E_G is the ambient band gap, E_{ex} is the exciton binding energy, ΔE_{dop} is the doping-induced band-gap narrowing, ΔE_{US}^k is the shift of the subbands in uniaxially strained GaP, and the k

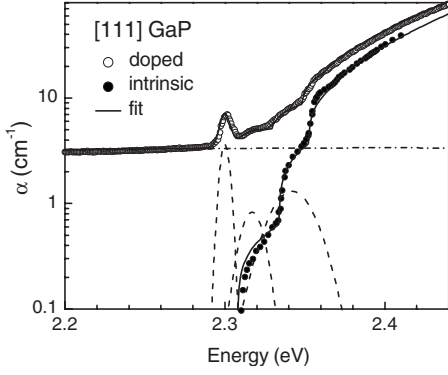


FIG. 10. Modeling (solid line) of [111] GaP:S spectra (open symbols) using the fit (solid line) of literature data for intrinsic absorption edge of GaP (solid symbols). The dash-dotted curve represents the absorption due to donor states. The dashed Gaussian peaks going from lower energies illustrate the S:BEx peak, the excited states of S:BEx complex, and the phonon replicas of S:BEx.

index refers to a particular transition. The \pm sign in the equation corresponds to phonon emission and absorption, respectively. The first term in Eq. (3) represents transition to a ground exciton state, while the second describes a band-to-band transition. The A_{ex}^p and A_{BB}^p coefficients account for the matrix elements at ambient pressure. The C_{ex}^k and C_{BB}^k coefficients were used to account for changes in absorption intensity under uniaxial strain; $C_{\text{ex}}^k = C_{\text{BB}}^k = 1$ at ambient pressure. Equation (3) neglects small effects such as transitions into excited excitonic states or the excitonic continuum, thermal broadening due to exciton-phonon interactions, and the temperature dependence of transition matrix elements.²⁹

In order to obtain the set of A_{ex}^p and A_{BB}^p constants, we modeled the published intrinsic absorption-edge spectrum of GaP at 77 K ($\Delta E_{\text{dop}} = \Delta E_{\text{US}}^k = 0$), shown by the black symbols in Fig. 10.³⁰ The solid line is a fit to the experimental data using the parameters listed in Table III. The values of A_{ex}^p and A_{BB}^p obtained were then applied to model the ambient absorption spectra of our doped GaP:S samples (open symbols in Fig. 10). We also adjusted the ΔE_{dop} values according to the relative shift of the observed S:BEx peaks, and reduced the exciton binding energy E_{ex} due to carrier-carrier screening effects (Table III). In addition to the intrinsic absorption given by Eq. (3), doped samples also had a constant absorption level due to the donor states (dash-dotted curve) and Gaussian peaks due to the S:BEx, their excited states and their phonon replicas (dashed curves).¹⁹ As discussed previously, these S:BEx peaks disappeared upon shock compression stresses greater than 1 GPa.

The polarization of transmitted light in our experiments was perpendicular to the direction of wave propagation. Under such conditions, all transitions I_k are allowed by symmetry.¹ In our model, each transition contributes to the absorption spectrum with an energy onset ΔE_{US}^k and relative strengths C_{ex}^k and C_{BB}^k for the excitonic and band-to-band components, respectively. Using the calculated values of ΔE_{US}^k (Fig. 2), in conjunction with the PL measurements, we obtained the C_{ex}^k and C_{BB}^k parameters by fitting to the absorption data. In the fitting procedure, we first adjusted the band-to-band components, starting from the lowest energy contri-

TABLE III. Parameters used in modeling the band-gap absorption of GaP.

Parameter	Value
E_G (at 85 K)	2.331 eV ^a
E_{TA}	12.8 meV ^a
E_{LA}	31.3 meV ^a
E_{TO}	46.5 meV ^a
E_{ex} (intrinsic and $2 \times 10^{15} \text{ cm}^{-3}$)	10 meV ^{a,b}
E_{ex} ($7-8 \times 10^{17} \text{ cm}^{-3}$)	4 meV
E_{ex} ($12 \times 10^{17} \text{ cm}^{-3}$)	3 meV
$A_{\text{ex}}^{\text{TA}}$	20 eV ^{-1/2} cm ⁻¹
$A_{\text{ex}}^{\text{LA}}$	50 eV ^{-1/2} cm ⁻¹
$A_{\text{ex}}^{\text{TO}}$	20 eV ^{-1/2} cm ⁻¹
$A_{\text{BB}}^p / A_{\text{ex}}^p$	55 eV ^{-3/2}
ΔE_{dop} ($2 \times 10^{15} \text{ cm}^{-3}$)	1 meV
ΔE_{dop} ($7-8 \times 10^{17} \text{ cm}^{-3}$)	6 meV
ΔE_{dop} ($12 \times 10^{17} \text{ cm}^{-3}$)	12 meV

^aDean *et al.* (Ref. 30).

^bRef. 31.

bution. The excitonic components were then added to complete the multicomponent fit. The C constants obtained are provided in Table IV. Our model assumes that changes in E_p and E_{ex} , expected to be on the order of few meV, are negligible.

V. DISCUSSION

The results for [111] oriented GaP:S are the most straightforward to interpret, due to the small number of transitions (Fig. 1). The band-to-band transitions, described by the coefficients C_{BB}^k and C_{BB}^k , are roughly constant up to the highest longitudinal stress (Table IV). The excitonic contributions of the same transitions C_{ex}^k and C_{ex}^k decrease substantially with stress. To illustrate this effect, spectra for [111] GaP:S are shown in Fig. 11, where the I_1 and I_2 transition thresholds are indicated by arrows. The lines in the figure show two types of fits: The curves labeled “BB” were generated using only the band-to-band contributions C_{BB}^k and C_{BB}^k , while the curves labeled “EX” were the best fits given equal excitonic and band-to-band contributions. It is clear that a nonzero excitonic component is required to model the shape of the 1 and 2.7 GPa spectra, while adding this part for the 5 GPa spectrum results in an overestimate of the absorption.

The excitonic reduction effect observed in [111] oriented GaP:S also occurs for [100] and [110] orientations, although these data are more complicated to interpret. For the [100] orientation, we resolved only the two lowest (I_1' and I_2') transitions at 2.7 GPa, and found that the single I_1' transition is sufficient to explain the spectral shape at 5 GPa. Nevertheless, none of these transitions showed the presence of excitons. For the [110] orientation, we observed two (I_1'' and I_2'') transitions at 2.7 GPa, while three (I_1'' , I_2'' , I_4'') transitions were detected at 4.3 GPa. All transitions resolved in the [110] absorption spectra showed the excitonic reduction effect.

TABLE IV. Coefficients C_{ex} and C_{BB} used to model the band-gap absorption in GaP shocked along different crystallographic axes.

Orientation	Longitudinal stress (GPa)	Shift of I_1 from PL data (meV)	Excitonic components (a.u.)	Band-to-band components (a.u.)	
[111]	1	-25 ± 2	$C_{\text{ex}}^I = 0.2 \pm 0.05$	$C_{\text{BB}}^I = 0.2 \pm 0.05$	
			$C_{\text{ex}}^J = 0.55 \pm 0.1$	$C_{\text{BB}}^J = 0.55 \pm 0.1$	
	2.7	-102 ± 2	$C_{\text{ex}}^I = 0.12 \pm 0.03$	$C_{\text{BB}}^I = 0.18 \pm 0.05$	
			$C_{\text{ex}}^J = 0.1 \pm 0.1$	$C_{\text{BB}}^J = 0.5 \pm 0.1$	
	5	-215 ± 2	$C_{\text{ex}}^I = 0 + 0.02$	$C_{\text{BB}}^I = 0.11 \pm 0.05$	
			$C_{\text{ex}}^J = 0.2 \pm 0.1$	$C_{\text{BB}}^J = 0.5 \pm 0.1$	
[100]	2.7	-162 ± 5	$C_{\text{ex}}^{I'} = 0.12 \pm 0.02$	$C_{\text{BB}}^{I'} = 0.12 \pm 0.02$	
			$C_{\text{ex}}^{J'} = 0 + 0.05$	$C_{\text{BB}}^{J'} = 0.1 + 0.05$	
	5	-310 ± 20	$C_{\text{ex}}^{I'} = 0.04 \pm 0.04$	$C_{\text{BB}}^{I'} = 0.09 \pm 0.01$	
			$C_{\text{ex}}^{J'} = 0 + 0.01$	$C_{\text{BB}}^{J'} = 0 + 0.02$	
	[110]	2.7	-102 ± 5	$C_{\text{ex}}^{I''} = 0.1 \pm 0.03$	$C_{\text{BB}}^{I''} = 0.1 \pm 0.03$
				$C_{\text{ex}}^{J''} = 0.1 \pm 0.1$	$C_{\text{BB}}^{J''} = 0.4 \pm 0.1$
4.3		-160 ± 20	$C_{\text{ex}}^{I''} = 0.05 \pm 0.05$	$C_{\text{BB}}^{I''} = 0.1 \pm 0.02$	
			$C_{\text{ex}}^{J''} = 0 + 0.1$	$C_{\text{BB}}^{J''} = 0.1 \pm 0.1$	
			$C_{\text{ex}}^{K''} = 0 + 0.2$	$C_{\text{BB}}^{K''} = 0.3 \pm 0.3$	

Indications of excitonic reduction for biaxial strains $< 1\%$ were reported in Ref. 2. The authors observed substantial broadening and eventual vanishing of fine exciton absorption peaks in the transitions related to the VB2 valence band. This effect was attributed to mixing of VB2 excitons with the quasicontinuum of excited states of VB1 excitons. The reduction of excitonic components detected for I_2 , I'_2 , and I''_2 transitions for strains $> 1\%$ in our work is consistent with such an effect. However, for uniaxial strains $> 2\%$, we also observe a substantial reduction in I_1 , I'_1 , and I''_1 excitonic

contributions, which originate from the VB1 band. This observation suggests that large anisotropic strains cause the dissociation of bound excitonic states. Another possibility is that Eq. (3), which is based on the assumption of parabolic bands near the band edges, may not accurately model the absorption data at large strains.

VI. CONCLUSIONS

The changes in the absorption spectra of GaP:S were observed, using time-resolved measurements in shock wave compression experiments. These results were modeled using the known deformation potentials in conjunction with PL measurements. At high uniaxial strains, the absorption and PL spectra indicate that the published deformation potentials overestimate the band-gap shifts. In addition, the set of coefficients that describe band-to-band transitions in GaP showed a substantial decrease in the intrinsic excitonic contribution to the absorption edge.

ACKNOWLEDGMENTS

The authors thank J. M. Winey for valuable discussions, and K. Zimmerman and K. Perkins for their help in performing the experiments. This work was supported by the DOE Grant No. DE-FG03-97SF21388.

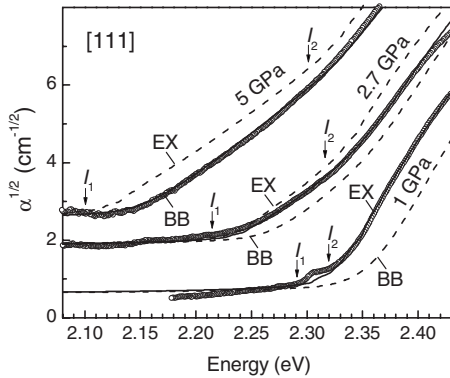


FIG. 11. The [111] GaP:S shock data (open symbols) at 1 GPa (sifted down by $1.5 \text{ cm}^{-1/2}$), 2.7 GPa, and 5 GPa (sifted up by $1.5 \text{ cm}^{-1/2}$) longitudinal stresses, and their respective fits including the intrinsic excitonic transitions (the “EX” labeled curves) or taking only the band-to-band contributions (the “BB” labeled curves).

- ¹H. Mathieu, P. Merle, E. L. Ameziane, B. Archilla, and J. Camassel, *Phys. Rev. B* **19**, 2209 (1979).
- ²R. G. Humphreys, U. Rossler, and M. Cardona, *Phys. Rev. B* **18**, 5590 (1978).
- ³W. Scott and J. R. Onffroy, *Phys. Rev. B* **13**, 1664 (1976).
- ⁴H. Mathieu, B. Archilla, P. Merle, and J. Camassel, *Phys. Rev. B* **20**, 4268 (1979).
- ⁵A. Onton and T. N. Morgan, *Phys. Rev. B* **1**, 2592 (1970).
- ⁶J. L. Merz, A. Baldereschi, and A. M. Sergent, *Phys. Rev. B* **6**, 3082 (1972).
- ⁷H. Mathieu, L. Bayo, J. Camassel, and P. Merle, *Phys. Rev. B* **22**, 4834 (1980).
- ⁸B. Gil, J. Camassel, J. P. Albert, and H. Mathieu, *Phys. Rev. B* **33**, 2690 (1986).
- ⁹A. R. Goni, K. Syassen, K. Strossner, and M. Cardona, *Phys. Rev. B* **39**, 3178 (1989).
- ¹⁰B. Gil, M. Baj, J. Camassel, H. Mathieu, C. Bonoita la Guillaume, N. Mestres, and J. Pascual, *Phys. Rev. B* **29**, 3398 (1984).
- ¹¹W. H. Gust and E. B. Royce, *J. Appl. Phys.* **42**, 1897 (1971).
- ¹²The VISAR measurement [L. M. Barker and R. E. Hollenbach, *J. Appl. Phys.* **43**, 4669 (1972)] of our [100] GaP:S sample showed elastic response of GaP up to 6 GPa.
- ¹³H. Y. Peng, M. D. McCluskey, Y. M. Gupta, M. Kneissl, and N. M. Johnson, *Phys. Rev. B* **71**, 115207 (2005).
- ¹⁴R. Zallen, and W. Paul, *Phys. Rev.* **134**, A1628 (1964).
- ¹⁵I. Balslev, *J. Phys. Soc. Jpn.* **21**, 101 (1966).
- ¹⁶R. Weil and W. O. Groves, *J. Appl. Phys.* **39**, 4049 (1968).
- ¹⁷A. Polian, and M. Grimsditch, *Phys. Rev. B* **60**, 1468 (1999).
- ¹⁸The existence of free carrier absorption in this spectral range is usually marked by the distinct λ^2 dependency, which in our case was detected only at energies less than 1.7 eV.
- ¹⁹P. J. Dean, *Phys. Rev.* **157**, 655 (1967).
- ²⁰A. J. Campillo and S. L. Shapiro, *IEEE J. Quantum Electron.* **QE-19**, 585 (1983).
- ²¹Y. M. Gupta, COPS code, SRI International, Menlo Park, CA, 1976 (unpublished). The shock velocity of GaP was approximated by its ambient sound speed (Ref. 17).
- ²²S. C. Jones, M. C. Robinson, and Y. M. Gupta, *J. Appl. Phys.* **93**, 1023 (2003).
- ²³S. C. Jones and Y. M. Gupta, *J. Appl. Phys.* **88**, 5671 (2000).
- ²⁴L. M. Barker and R. E. Hollenbach, *J. Appl. Phys.* **41**, 4208 (1970).
- ²⁵For visual purposes, in Fig. 6 the stress curve calculated in the middle of sample is shifted in time to correspond to the impact moment.
- ²⁶D. R. Wight, *J. Phys. D* **10**, 431 (1977).
- ²⁷G. G. Macfarlane, T. P. McLean, J. E. Quarrington, and V. Roberts, *Phys. Rev.* **111**, 1245 (1958).
- ²⁸T. P. McLean, *Prog. Semicond.* **5**, 53 (1960).
- ²⁹R. Corkish and M. A. Green, *J. Appl. Phys.* **73**, 3988 (1993).
- ³⁰P. J. Dean and D. G. Thomas, *Phys. Rev.* **150**, 690 (1966).
- ³¹It has been argued that exciton binding energies of up to 22 meV are possible for intrinsic GaP [M. D. Sturge, A. T. Vink, and F. P. J. Kuipers, *Appl. Phys. Lett.* **32**, 49 (1978)], though these values would be considerably smaller for doped GaP.